Similarity and singularity in adhesive elastohydrodynamic touchdown

Andreas Carlson and L. Mahadevan

Citation: Physics of Fluids **28**, 011702 (2016); doi: 10.1063/1.4938115
View online: http://dx.doi.org/10.1063/1.4938115
View Table of Contents: http://scitation.aip.org/content/aip/journal/pof2/28/1?ver=pdfcov
Published by the AIP Publishing

PHYSICS OF FLUIDS **28**, 011702 (2016)

Similarity and singularity in adhesive elastohydrodynamic touchdown

Andreas Carlson[1,2,a)] and L. Mahadevan[2,3,b)]
[1]*Mechanics Division, Department of Mathematics, University of Oslo, Oslo 0316, Norway*
[2]*Paulson School of Engineering and Applied Sciences and Wyss Institute for Biologically Inspired Engineering, Harvard University, Cambridge, Massachusetts 02138, USA*
[3]*Kavli Institute for Bionano Science and Technology, Departments of Physics, and Organismic and Evolutionary Biology, Harvard University, Cambridge, Massachusetts 02138, USA*

(Received 15 July 2015; accepted 24 November 2015; published online 5 January 2016)

We consider the dynamics of an elastic sheet as it starts to adhere to a wall, a process that is limited by the viscous squeeze flow of the intervening liquid. Elastohydrodynamic lubrication theory allows us to derive a partial differential equation coupling the elastic deformation of the sheet, the microscopic van der Waals adhesion, and viscous thin film flow. We use a combination of numerical simulations of the governing equation and a scaling analysis to describe the self-similar touchdown of the sheet as it approaches the wall. An analysis of the equation in terms of similarity variables in the vicinity of the touchdown event shows that only the fundamental similarity solution is observed in the time-dependent numerical simulations, consistent with the fact that it alone is stable. Our analysis generalizes similar approaches for rupture in capillary thin film hydrodynamics and suggests experimentally verifiable predictions for a new class of singular flows linking elasticity, hydrodynamics, and adhesion. © *2016 AIP Publishing LLC*. [http://dx.doi.org/10.1063/1.4938115]

The onset of adhesion between a thin sheet or membrane and a solid surface in a fluid environment is a common paradigm in many situations in microfluidics, coating, and food processing; for example, it is critical for initiation of intercellular signaling[1] and for the formation of elastic bonding in engineering applications, e.g., wafer bonding.[2] A minimal description of the process requires us to couple the elastic interface deformation, the microscopic adhesion physics, and the viscous flow between the two solid surfaces, and can lead to diverging velocity gradients or geometric singularities.[3–5] Indeed, analogs of these flows have been well studied in the context of the rupture of capillary thin fluid films on substrates[6–15] that reveal a finite–time singularity.[10,11]

Our analysis focuses on small scale flows wherein inertial effects in the fluid and the sheet may be neglected. Initially, we consider the touchdown of a long and wide elastic sheet with a length L, which is initially separated from a solid substrate by a thin viscous fluid film of viscosity μ and height $\hat{h}(\hat{x},\hat{t})$, focusing on the two-dimensional situation, although we will eventually also treat the three dimensional case that might be easier to realize experimentally. The sheet starts to move towards the wall owing to a van der Waals adhesion potential (Fig. 1(a)). Mechanical equilibrium of the sheet is determined by the balance of transverse forces that reads[16]

$$\hat{p}(\hat{x},\hat{t}) = B\hat{h}_{\hat{x}\hat{x}\hat{x}\hat{x}}(\hat{x},\hat{t}) + \frac{A}{3\hat{h}^3(\hat{x},\hat{t})}, \tag{1}$$

where $\hat{p}(\hat{x},\hat{t})$ is the fluid pressure, $B\hat{h}_{\hat{x}\hat{x}\hat{x}\hat{x}}(\hat{x},\hat{t})$ is the elastic bending pressure due to long wavelength deformations of the sheet with bending stiffness B [N · m], and $\frac{A}{3\hat{h}^3(\hat{x},\hat{t})}$ is the van der

a)Electronic mail: acarlson@math.uio.no
b)Electronic mail: lm@seas.harvard.edu

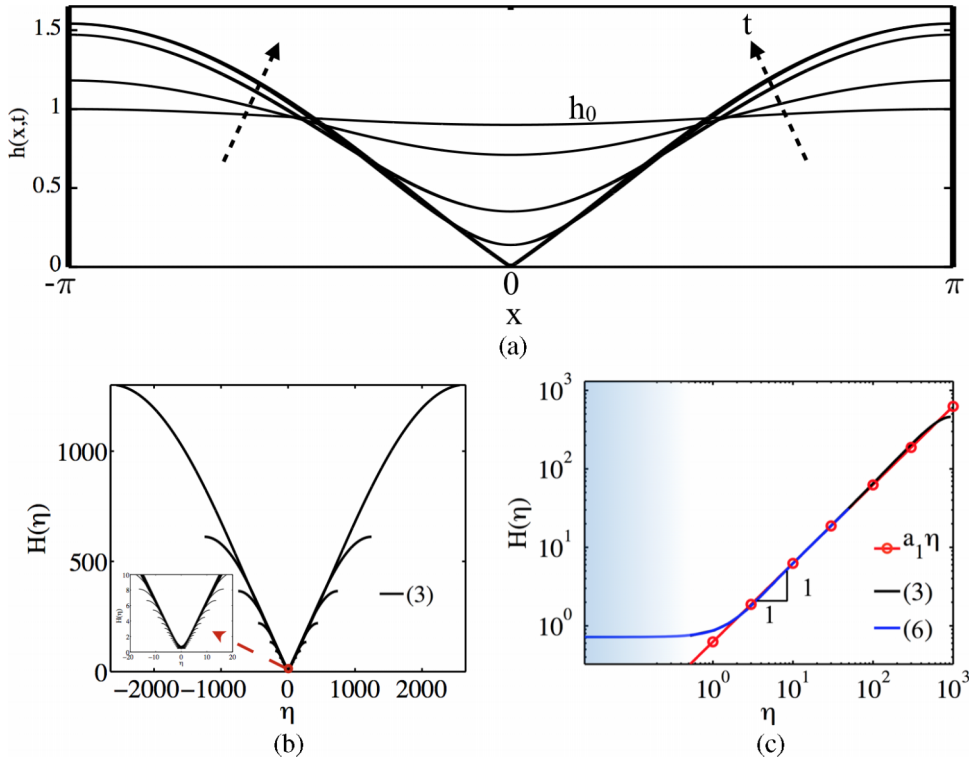

FIG. 1. (a) Numerical simulations of (3) for the dynamics of touchdown showing the evolution of the sheet at five different time points $t = [0,\ 6.50,\ 7.98,\ 8.08,\ 8.09]$. The sheet is initialized with $h_0 = h(x,0) = 1 - 0.05\times(1+\cos(x))$ and is seen to adopt a wedge-like profile as $t \to t_C$ for $x \in [-2.5\ 2.5]$. Our simulations suggest that the contact point $x_C = 0$ and the contact time $t_C = 8.0899$. (b) The shapes obtained by solving (3) may be collapsed onto a universal self-similar shape by using the rescaled variables $H(\eta) = h(x,t)/(t_C - t)^{\frac{1}{3}}$, $\eta = (x - x_C)/(t_C - t)^{\frac{1}{3}}$, over more than two orders of magnitude in $H(\eta)$ and η. The inset in the lower left shows the self-similar collapse for $\eta \in [-20\ 20]$. (c) The rescaled height $H(\eta)$ obtained by solving the PDE (3) and the similarity ODE (6) and (7) (with $m = 1$) shows that the height profiles adopt a shape $H(\eta) = a_1\eta$ as $|\eta| \to \infty$ (red circle). The shaded area $\eta \le 1$ illustrates the inner region near the contact point where the shape of the sheet arises from the balance between viscous forces, van der Waals adhesion pressure, and elastic bending resistance.

Waal adhesion pressure[17] with A [N · m] the Hamaker constant. Here, and elsewhere, the subscript denotes derivative i.e., $(\cdot)_{\hat{x}} = \partial(\cdot)/\partial\hat{x}$. Furthermore, we have assumed that the scaled fluid film thickness $\hat{h}(\hat{x},\hat{t})/L \ll 1$ and that the elastic sheet has a small slope, $\hat{h}_{\hat{x}}(\hat{x},\hat{t}) \ll 1$.

As the sheet approaches the substrate, the intervening fluid is squeezed out, leading to non-uniform deformations of the sheet. We assume that there is no-slip of the fluid at both surfaces and that viscous forces dominate over inertial effects. By using the lubrication approximation for the description of the fluid motion,[18] we obtain an evolution equation for the film height $\hat{h}(\hat{x},\hat{t})$ given by

$$\hat{h}_{\hat{t}}(\hat{x},\hat{t}) = \left(\frac{\hat{h}^3(\hat{x},\hat{t})}{12\mu}\hat{p}_{\hat{x}}(\hat{x},\hat{t})\right)_{\hat{x}} = \left(\frac{\hat{h}^3(\hat{x},\hat{t})}{12\mu}\left(B\hat{h}_{\hat{x}\hat{x}\hat{x}\hat{x}}(\hat{x},\hat{t}) + \frac{A}{3\hat{h}^3(\hat{x},\hat{t})}\right)_{\hat{x}}\right)_{\hat{x}}. \tag{2}$$

The sixth order nonlinear partial differential equation (2) couples the dynamics of the elastic sheet, the viscous forces in the lubricating film, and the destabilizing intermolecular adhesion pressure. To simplify the parameter dependence of the solutions to this equation, we scale the variables appearing in (2) as; $\hat{x} = x\ell = x\hat{h}_0(B/A)^{\frac{1}{4}}$, $\hat{h}(x,t) = \hat{h}_0 h(x,t)$ and $\hat{t} = \tau t = \frac{12\hat{h}_0\ell^2\mu}{A}t$, where $\tau = \frac{12\hat{h}_0\ell^2\mu}{A}$. Introducing these scaled variables into (2) gives us the parameter free dimensionless elastohydrodynamic lubrication equation,

$$h_t(x,t) = \left(h^3(x,t)h_{xxxxx}(x,t) - \frac{h_x(x,t)}{h(x,t)}\right)_x. \tag{3}$$

Completing the formulation of the initial value problem requires an initial condition which we assume is given by a perturbed flat profile $h_0 = h(x,t=0) = 1 - 0.05 \times (1 + \cos(x))$ with the minimum initial film height located at $x = 0$, and six boundary conditions at the ends. Assuming that the touchdown region $x = x_C$, $t \to t_C$ is far from the boundary, we use periodic conditions at the two ends of the sheet, with vanishing odd derivatives i.e., $h_x(x,t)|_{x=\pm\pi} = h_{xxx}(x,t)|_{x=\pm\pi} = h_{xxxxx}(x,t)|_{x=\pm\pi} = 0$.

The dispersion relation of linearized version of (3) can be obtained by substituting $h(x,t) = h_0(1 + \epsilon \exp(\lambda t + ikx))$ in (3), ($\epsilon \ll 1$) with k the wave number, h_0 the initial film height and we find that the growth rate $\lambda = \frac{k^2}{h_0}(1 - (h_0 k)^4)$. Thus, we see that the elastic thin film is only unstable for long wavelength perturbations $h_0 k < 1$, similar to what is known in capillary dominated flows. This suggests that when we solve (3) numerically with $h_0 \approx 1$, a minimal domain size $x \geq 2\pi/k_c$ is required, with $k_c = 1$ the critical wave number.

We solve (3) using a second order finite difference discretization in space and a Gear method[19] for time stepping. In Fig. 1(a), we plot the evolution of the shape of the sheet and see that the solution appears to adopt a self-similar shape in the neighborhood of the touchdown point $x = x_C = 0$, $t = t_C$, where the contact time t_C is defined as the last time point before $h(x,t) \leq 0$, when the numerics also breaks down.

Inspired by the apparent self-similar shape of the sheet as $h(x \to x_C, t \to t_C) \to 0$, we look for a self-similar solution of (3) to understand the scaling behavior of the sheet in the immediate vicinity of touchdown. Adopting the similarity ansatz,

$$h(x,t) = (t_C - t)^{\alpha} H(\eta), \quad \eta = \frac{x - x_C}{(t_C - t)^{\beta}}, \tag{4}$$

with $H(\eta)$ the scaled height, η the similarity variable, and inserting (4) into (3) we get

$$(t - t_C)^{\alpha - 1}(\alpha H(\eta) - \beta \eta H'(\eta)) = \left((t - t_C)^{4\alpha - 6\beta} H(\eta)^3 H'''''(\eta) - (t - t_C)^{-2\beta} \frac{H'(\eta)}{H(\eta)}\right)', \tag{5}$$

with $H'(\eta) \equiv \partial H(\eta)/\partial \eta$. Equating the exponents appearing on both sides of the equation, we find that $\alpha - 1 = 4\alpha - 6\beta = -2\beta$ so that $\alpha = \beta = 1/3$. To test the self-similar scaling ansatz (4) with $\alpha = \beta = 1/3$, we re-plot the results obtained by solving the partial differential equation (3) in Fig. 1(a) using the ansatz (4). In Fig. 1(b), we see that the solution of (3) converges rapidly to a self-similar form $H(\eta)$ over many orders of magnitude in η, confirming the validity of our similarity hypothesis.

Inserting this result in (5), we find that the similarity variable $H(\eta)$ satisfies the ordinary differential equation (ODE)

$$\frac{1}{3}(H(\eta) - \eta H'(\eta)) = \left(H^3(\eta) H'''''(\eta) - \frac{H'(\eta)}{H(\eta)}\right)'. \tag{6}$$

Since the similarity solution of partial differential equation (3) is well described by (6), a natural question is if we can solve this latter equation directly and determine the self-similar shape associated with the touchdown event. This requires that we supplement (6) with a set of boundary conditions. Noting that numerical solution of (3) in Fig. 1(a) is symmetric around the contact point $\eta = 0$ suggests that odd derivatives of the solution vanish, i.e., $H'(0) = H'''(0) = H'''''(0) = 0$. Furthermore, since the sheet height changes rapidly near the contact point, i.e., $x = x_C$, $t \to t_C$, the far-field is quasi-static by comparison, i.e., $h_t \approx 0$.[10,11] Thus, we expect that the far-field solution is independent of the evolution of the singularity as $t \to t_C$. This translates into a far-field Robin boundary condition that in similarity variables reads as

$$\frac{1}{3}(H(\eta) - \eta H'(\eta)) \to 0, \ as \ |\eta| \to \infty. \tag{7}$$

We immediately see that the far-field solution is satisfied by $H(\eta) = a\eta + C$ as $|\eta| \to \infty$, and the integration constant $C = 0$ for consistency. Plotting the results of the numerical solution of (3) shown in Fig. 1(a) in terms of the rescaled height $H(\eta)$ as $t \to t_C$ in logarithmic coordinates (Fig. 1(c)) confirms that $H(\eta) \sim \eta$ over a wide range of η. The constant a corresponds

TABLE I. Discrete solutions of self-similar ODE (6)-(7) showing the values $a_m, H_m(0), H_m''(0), H_m''''(0)$. Comparison of these values with those obtained from the solution of PDE (3) show that it is consistent only with the fundamental self-similar solution $H_1(\eta)$.

m	a_m	$H_m(0)$	$H_m''(0)$	$H_m''''(0)$
PDE (3)	...	0.708	0.324	−0.183
1	0.625	0.719	0.321	−0.186
2	0.290	0.452	0.031	0.190
3	0.193	0.338	0.051	−0.099
4	0.147	0.283	0.0215	0.068
5	0.119	0.245	0.0223	−0.034

to an asymptotic matching condition for the far-field associated with (6), so that all together $H'(\infty) = a$, $H''(\infty) = H'''(\infty) = H''''(\infty) = 0$, along with the symmetry conditions at $\eta = 0$ complete the formulation of the boundary value problem for $H(\eta)$ that satisfies (6).

We solve the self-similar ODE ((6) and (7)) with the finite-difference-based boundary value solver BVP4C in Matlab[20] on a finite size domain $\eta = 50$, with the boundary conditions; $H'(0) = H'''(0) = H'''''(0) = H''(50) = H'''(50) = H''''(50) = 0$, $H'(50) = a$, noting that our results are insensitive to changes in domain size. We find that we get a discrete family of solutions for (6)-(7) (Table I) denoted by the subscript m with

$$H(\eta) \equiv H_m(\eta), \qquad a \equiv a_m. \tag{8}$$

To determine them, our numerical procedure starts with an initial guess for the height in the vicinity of contact $H_0(0)$, together with a guess of the initial solution $H_0(\eta) = H_0(0) + a_0\eta$. We systematically vary the initial guesses $H_0(0)$ and a_0, allowing us to identify the first thirteen solutions $m = 1, 2, \ldots, 13$ for $H_m(\eta)$ satisfying (6) and (7). In Fig. 2(a) and Table I, a comparison of these solutions of ODE (6) and (7) with the solution of the time-dependent partial differential equation (3) shows that only the fundamental solution associated with $m = 1$ agrees with the solution of complete PDE (3), a scenario also seen for capillary film rupture[9,11,12,14] and justified using a stability analysis in similarity coordinates. A qualitative explanation of why this is so follows by noting that solutions of (6) and (7) with $m \neq 1$ has multiple minima in the height h; any perturbation will cause one of them to be lower, and run away dynamically from the others, and thus eventually end up locally like the fundamental discrete solution with $m = 1$. To test this, we use time-dependent solution of (3) to evolve these self-similar solutions, using $H_m(\eta)$ as the initial condition for the time dependent PDE (3). In Fig. 2(b), we show the result of our simulation of (3) with $h(x,0) = H_m(\eta)$, $m = 3$. The position x_C and time t_C of contact shifts and similar results arise for all values of $m > 1$. Similar observations have been made for capillary thin film rupture.[9] Rescaling the results with (4) shows that the solution converges to that associated with the shape of the fundamental solutions $m = 1$ in the vicinity of touchdown (Fig. 2(c)).

Having analyzed the two-dimensional problem, we now turn to the three-dimensional version of touchdown, which in the lubrication approximation is governed by the two-dimensional version of (3),

$$h(x,y,t)_t - \nabla \cdot \left(h^3(x,y,t) \nabla \left(\nabla^4 h(x,y,t) + \frac{1}{3h^3(x,y,t)} \right) \right) = 0, \tag{9}$$

where ∇ is the two-dimensional gradient operator. We solve the partial differential equation (9) numerically by using an adaptive finite-element method[21,22] after the sheet is initialized with a constant height that has an axisymmetric perturbation at the center of the domain. In Fig. 3(a), we show that the three dimensional shape of the sheet is axially symmetric near the contact region. Noting that this solution also has the same scaling structure as the planar problem, we test the self-similar scaling ansatz $h(x,y,t) = (t_C - t)^{1/3} H(\eta)$ with $\eta = (r - r_C)/(t_C - t)^{1/3}$, where $r^2 = x^2 + y^2$ and r_C is the contact position, by plotting the numerical height profile in Fig. 3(a) along a plane that goes

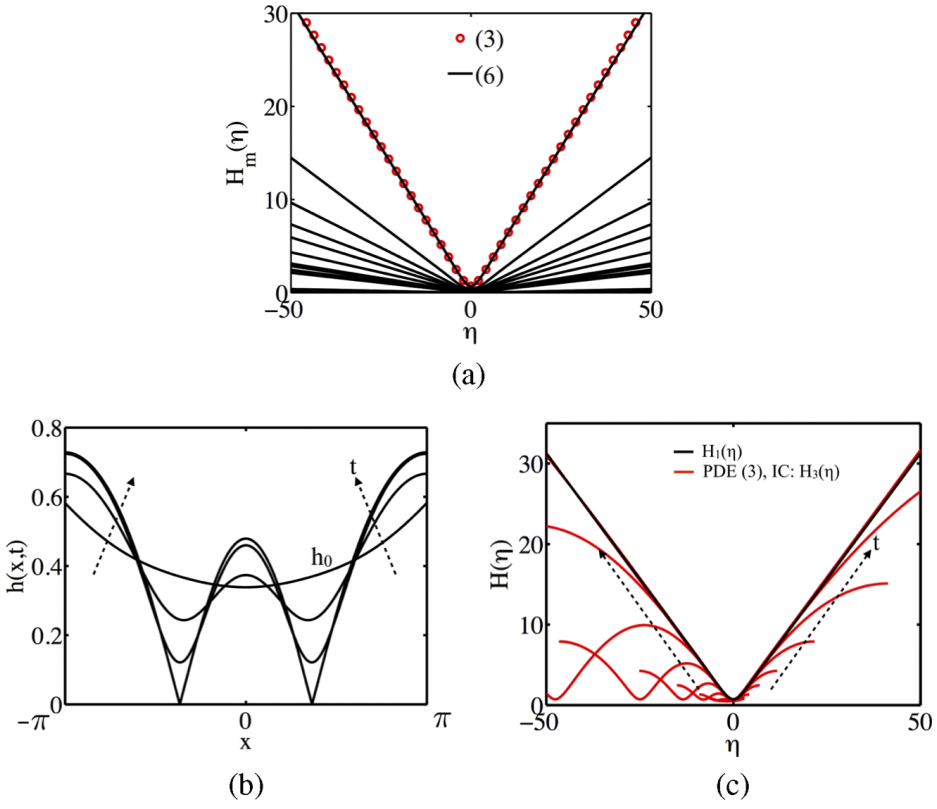

FIG. 2. Comparison between the self-similar shape of the sheet predicted by time-dependent PDE (3) and the first thirteen solutions $H_m(\eta); m \in [1-13]$ of the similarity ODE (6) and (7). We note that only the fundamental solution $H_1(\eta)$ of (6) and (7) is consistent with that of the PDE (3) (red circle). (b) Numerical simulations of the PDE (3) using the initial condition associated with the self-similar shape $h_0(x, t=0) = H_3(\eta)$ shows the evolution of the shape of the sheet for four different time points $t = [0,\ 0.28,\ 0.336,\ 0.341]$. We find that the numerically measured contact time is $t_C = 0.3412$ and the contact points are $x_C = [-1.48, 1.48]$. (c) By using the rescaled variables $H(\eta) = h(x,t)/(t_C - t)^{\frac{1}{3}}$, $\eta = (x - x_C)/(t_C - t)^{\frac{1}{3}}$ with $x_C = 1.48$ corresponding to the contact on the right side, we see that the shapes of the sheet obtained in Fig. 2(b) collapse onto the universal shape of the fundamental solution of (6) and (7) $H_1(\eta)$ (shown in black). The deviations away from the contact point are due to the effects of the second touchdown at $x_C = -1.48$.

through the origin. In Fig. 3(b), we see that solution of (9) converges rapidly to the self-similar form $H(\eta)$, confirming our similarity hypothesis. Plotting the result of the numerical solution of (9) shown in Fig. 3(a) in terms of the rescaled height $H(\eta)$ as $t \to t_C$ in logarithmic coordinates (Fig. 3(c)) confirms that $H(\eta) \sim \eta$ over a wide range of η. We note that the asymptotic matching condition a is different for the two-dimensional (2D) simulation compared to the one-dimensional (1D) simulation.

We conclude with a few remarks on the approximations inherent in our approach, associated with using a continuum theory for the fluid that neglects molecular and inertial effects, and an elastic plate theory that neglects three-dimensional effects. Our simulations show that the sheet converges to the self-similar shape relatively quickly, when the scaled height $h(x,t) \approx 0.3$ (Fig. 1(b)). Choosing a typical value for the initial height of the fluid film to be $\hat{h}_0 = 300$ nm suggests that by this time the height dips down to ≈100 nm, much larger than molecular dimensions, so that a continuum theory should remain valid. During touchdown, the horizontal scale over which the deformation varies is given by $\ell(t) = h_{min}(t)(B/A)^{\frac{1}{4}}$. Since $h_x \sim h_{min}(t)/\ell(t) \sim (A/B)^{\frac{1}{4}} \ll 1$ because $B \gg A$, ($A = 10^{-20}$ N · m, $B = 1$ N · m), the two-dimensional plate theory that we have used here remains reasonable and does not have to be replaced by a three-dimensional theory. Finally, as the sheet and fluid velocity diverges near contact, inertial effects can become important, particularly as the reduced Reynolds number $Re \equiv \frac{\rho U h_0^2}{L\mu} \sim (t_C - t)^{-\frac{1}{3}}$ is also singular as $t \to t_C$. By

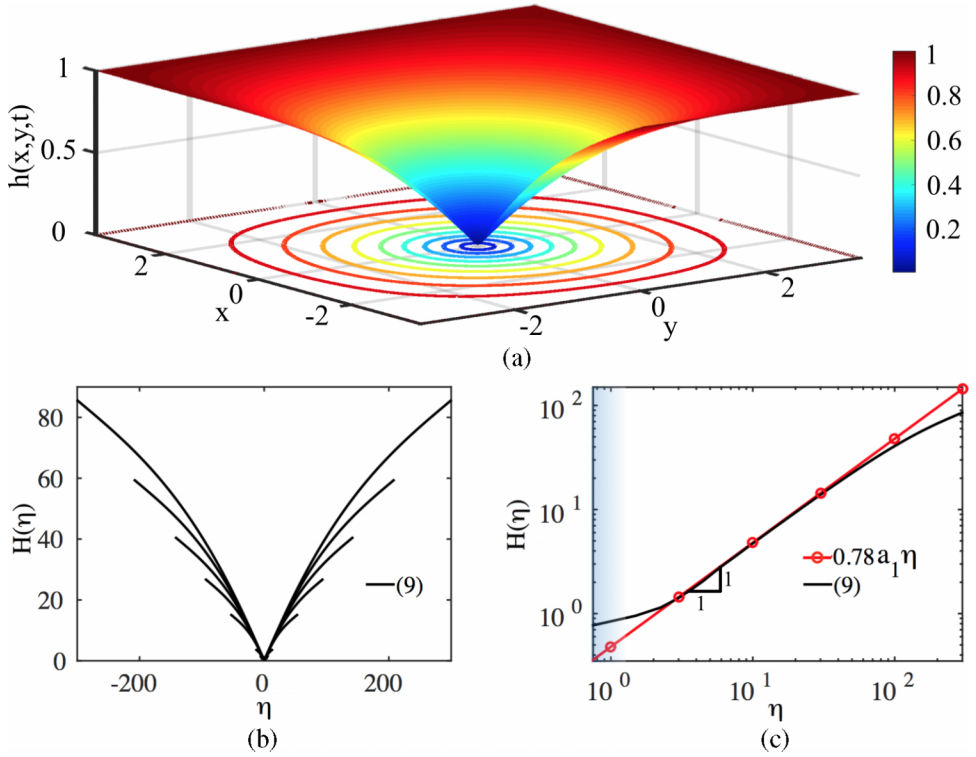

FIG. 3. (a) Numerical simulation of (9) for the dynamics of touchdown shown just before touchdown at $x_C = y_C = 0$ associated with a scaled time $t = 5.26$. The sheet is initialized with $h_0 = h(r,0) = 1 - 0.1 \times (\tanh(r^2/2) - 1.0)$ and is seen to adopt a conical profile as $t \to t_C$ for $x \in [-2.5\ 2.5]$, $y \in [-2.5\ 2.5]$, where $r^2 = x^2 + y^2$. Our simulation allows us to measure the contact time $t_C = 5.2622$ with the following conditions imposed at the boundaries; $\nabla^2 h \cdot \mathbf{n} = \nabla p \cdot \mathbf{n} = 0$, $h(x,y,t) = 1.0$. (b) The shapes obtained by solving (9) may be collapsed onto a universal self-similar shape by using the rescaled variables $H(\eta) = h(r,t)/(t_C - t)^{\frac{1}{3}}$, $\eta = (r - r_C)/(t_C - t)^{\frac{1}{3}}$, over more than two orders of magnitude in $H(\eta)$ and η. (c) The rescaled height $H(\eta)$ obtained by solving PDE (9) shows that the height profiles adopt a shape $H(\eta) = 0.48\eta$ as $|\eta| \to \infty$ (red circle). The shaded area $\eta \leq 1$ illustrates the inner region near the contact point where the shape of the sheet arises from the balance between viscous forces, van der Waals adhesion pressure, and elastic bending resistance.

assuming $Re \approx O(1)$, we get a scaling estimate for the height at which inertia becomes significant $\hat{h}_I \sim \frac{\rho A^{\frac{3}{2}}}{12 B^{\frac{1}{2}} \mu^2}$; for $\mu = 10^{-3}$ Pa · s, $\rho = 10^3$ kg/m^3, we find that $\hat{h}_I < 2.5$ Å so that the approximation of neglecting inertial effects remains valid.

All together, our analysis reveals a new class of singular flows linking elasticity, hydrodynamics and adhesion, relevant to contact between a thin elastic sheet and an adherent surface. A combination of numerical simulations and similarity analysis shows that the height and deformation of the sheet has a simple power law form. Analysis of the governing equations in similarity coordinates further allows us to determine the universal self-similar shape of the elastic sheet in the neighborhood of touchdown. A qualitative analysis of the discrete set of self-similar film shapes shows that the fundamental solution alone is consistent with the time-dependent numerical simulation. A natural next step is to experimentally test the regime of applicability of our results, particularly since they are well within the scope of methods such as total internal reflection microscopy imaging that can visualize the wedge-like (or conical) profiles associated with contact.

We would like to thank C. N. Kaplan for stimulating discussions, the anonymous reviewers for their comments that improved the manuscript, and NSF DMR 14-20570 and NSF IOS 12-57946 for partial financial support.

[1] P. Bongrand, *Physical Basis for Cell Adhesion* (CRC Press, 1988).
[2] F. Rieutord, B. Bataillou, and H. Moriceau, "Dynamics of a bonding front," Phys. Rev. Lett. **94**, 236101 (2005).

[3] G. I. Barenblatt, *Similarity, Self-Similarity, and Intermediate Asymptotics* (Consultants Bureau, 1979).
[4] J. Eggers, "Nonlinear dynamics and breakup of free-surface flows," Rev. Mod. Phys. **69**, 865–929 (1997).
[5] J. Egger and M. A. Fontelos, "The role of self-similarity in singularities of partial differential equations," Nonlinearity **22**, R1–R44 (2009).
[6] R. K. Jain and E. Ruckstein, "Stability of stagnant viscous films on a solid surface," J. Colloid Interface Sci. **54**, 108–116 (1976).
[7] M. B. Williams and S. H. Davis, "Non-linear theory of film rupture," J. Colloid Interface Sci. **99**, 220–228 (1982).
[8] J. P. Bruelbacht, S. G. Bankoff, and S. H. Davis, "Nonlinear stability of evaporating/condensing liquid films," J. Fluid Mech. **195**, 463–494 (1988).
[9] A. J. Bernoff, A. L. Bertozzi, and T. P. Witelski, "Axisymmetric surface diffusion: Dynamics and stability of self-similar pinchoff," J. Stat. Phys. **93**, 725–776 (1998).
[10] W. Zhang and J. R. Lister, "Similarity solutions for van der Waals rupture of a thin film on a solid substrate," Phys. Fluids **11**, 2454–2462 (1999).
[11] T. P. Witelski and A. J. Bernoff, "Stability of self-similar solutions for Van der Waals driven thin film rupture," Phys. Fluids **11**, 2443–2445 (1999).
[12] T. P. Witelski and A. J. Bernoff, "Dynamics of three-dimensional thin film rupture," Physica D **147**, 155–176 (2000).
[13] D. Vaynblat, J. R. Lister, and T. P. Witelski, "Rupture of thin viscous films by van der Waals forces: Evolution and self-similarity," Phys. Fluids **13**, 1130–1140 (2001).
[14] A. J. Bernoff and T. P. Witelski, "Stability and dynamics of self-similarity in evolution equations," J. Eng. Math. **66**, 11–31 (2010).
[15] R. V. Craster and O. K. Matar, "Dynamics and stability of thin liquid films," Rev. Mod. Phys. **81**, 1131–1198 (2009).
[16] L. D. Landau and E. M. Lifshitz, *Theory of Elasticity* (Elsevier, 1986).
[17] J. N. Israelachvili, *Intermolecular and Surface Forces*, 3rd ed. (Elsevier, 2011).
[18] G. K. Batchelor, *An Introduction to Fluid Dynamics* (Cambridge University Press, 1967).
[19] C. W. Gear, "Simultaneous numerical solution of differential-algebraic equations," IEEE Trans. Circuit Theory **18**, 89–95 (1971).
[20] MATLAB version 8.2.0.701 (R2013b), The MathWorks, Inc., Natick, MA, 2013, Vol. 49.
[21] G. Amberg, R. Tönhardt, and C. Winkler, "Finite element simulations using symbolic computing," Math. Comput. Simul. **49**, 257–274 (1999).
[22] A. Carlson and L. Mahadevan, "Elastohydrodynamics and kinetics of protein patterning in the immunological synapse," PLoS Comput. Biol. (in press).